International Journal of Biological Macromolecules 277 (2024) 134493

Contents lists available at ScienceDirect

International Journal of Biological Macromolecules

journal homepage: www.elsevier.com/locate/ijbiomac

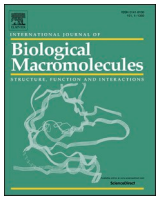

Structurally decoupled hyaluronic acid hydrogels for studying matrix metalloproteinase-mediated invasion of metastatic breast cancer cells

Kasra Goodarzi, Shreyas S. Rao *

Department of Chemical and Biological Engineering, The University of Alabama, Tuscaloosa, AL 35487, USA

ARTICLE INFO

Keywords:
Hyaluronic acid
Hydrogel
Invasion
Crosslinking
Breast cancer metastasis
Spheroids

ABSTRACT

In recent years, polymeric hydrogels have been employed to investigate cancer cell-extracellular matrix (ECM) interactions *in vitro*. In the context of breast cancer, cancer cells are known to degrade the ECM using matrix-metalloproteinases (MMPs) to support invasion resulting in disease progression. Polymeric hydrogels incorporating MMP-cleavable peptides have been employed to study cancer cell invasion, however, the approaches employed to incorporate these peptides often change other hydrogel properties. This underscores the need for decoupling hydrogel properties while incorporating MMP-cleavable peptides. Herein, we report structurally decoupled hyaluronic acid (HA) hydrogels formulated using varying ratios of a biologically sensitive MMP-cleavable peptide and an insensitive counterpart (Dithiothreitol (DTT) or polyethylene glycol dithiol (PEGDT)) to study MMP-mediated metastatic breast cancer cell invasion. Rheological, swelling ratio, estimated mesh size, and permeability measurements showed similar mechanical and physical properties for hydrogels crosslinked with different DTT (or PEGDT)/MMP ratios. However, their degradation rate in the presence of collagenase correlated with the ratio of MMP-cleavable peptide. Encapsulated metastatic breast cancer spheroids in HA hydrogels with MMP sensitivity exhibited increased invasiveness compared to those without MMP sensitivity after 14 days of culture. Overall, such structurally decoupled HA hydrogels provide a platform to study MMP-mediated breast cancer cell invasion *in vitro*.

1. Introduction

Polymeric hydrogels have been extensively employed to study tumor cell-matrix interactions as they provide tumor cells with a relevant three dimensional (3D) context evidenced *in vivo* and enabling us to maintain the cellular phenotype *in vitro* [1–4]. The hydrophilic nature of hydrogels enables them to absorb large amounts of water, recapitulating the elastic and viscoelastic properties of the extracellular matrix (ECM), along with its composition [5–8]. In addition, the ability to tune hydrogel properties has enabled recapitulation of several key aspects of the tumor microenvironment *in vitro*. For instance, it is well known that the tumor microenvironment provides biophysical and biochemical cues, that can independently modulate cancer cell phenotype [9–12]. Polymeric hydrogels provide the ability to recapitulate these cues and subsequently study how these cues influence tumor cell phenotypes in an *in vitro* setting [13]. To this end, both natural (e.g., hyaluronic acid (HA), collagen) and synthetic (e.g., polyethylene-glycol (PEG)) hydrogels have been employed to study cancer cell-matrix interactions, including how biophysical cues such as matrix stiffness, and biochemical cues such as incorporation of adhesion or degradation cues influence cancer cell fate [14–19].

In the context of breast cancer, it is well known that the cancer cells invade the tissue at the primary and metastatic sites by degrading the native ECM with matrix-metalloproteinases (MMPs), leading to disease progression [20–22]. MMPs are a group of zinc-dependent endopeptidases that can degrade almost every component of the ECM, which is required for tumor cell migration and invasion. MMPs are not only produced by tumor cells, but also by stromal cells in the tumor microenvironment, highlighting the complex interactions that contribute to tumor progression [23,24]. Consequently, efforts have been made to model MMP-mediated invasion of breast cancer cells *in vitro*. Collagen-based hydrogels have been used to study the invasion of breast cancer cells and spheroids [25,26]. However, decoupling of hydrogel properties is typically challenging as change in one property can simultaneously change other properties. Another approach involves incorporating MMP-cleavable crosslinks into the hydrogel structure via the utilization of multiple crosslinking strategies. This approach has been employed in HA as well as PEG based hydrogel systems to study invasion in breast

* Corresponding author.
E-mail address: srao3@eng.ua.edu (S.S. Rao).

https://doi.org/10.1016/j.ijbiomac.2024.134493
Received 13 March 2024; Received in revised form 19 July 2024; Accepted 2 August 2024
Available online 5 August 2024

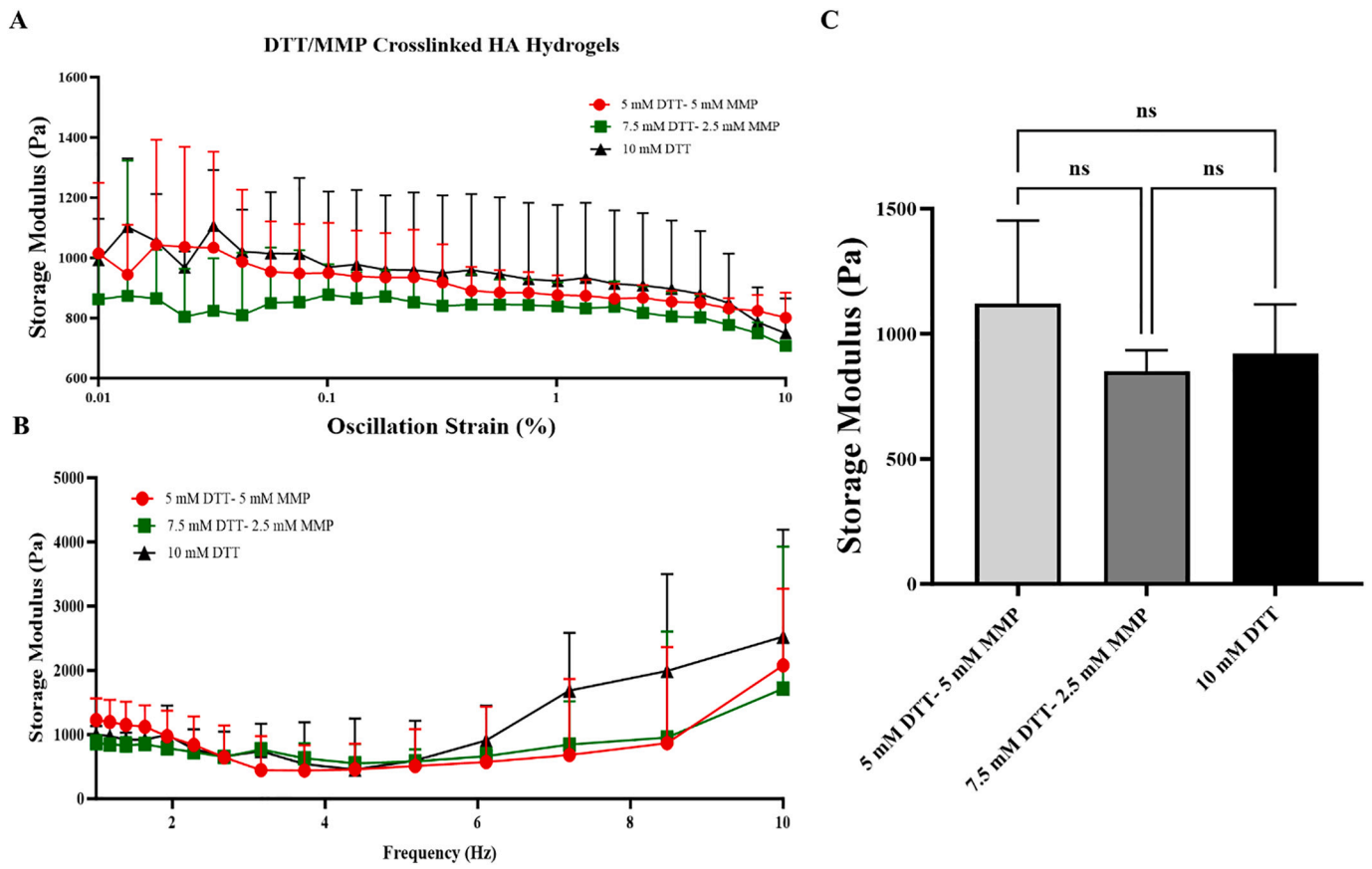

Fig. 1. Mechanical characterization of DTT/MMP crosslinked HA hydrogels. (A) Storage modulus of DTT/MMP crosslinked HA hydrogels as a function of oscillation strain (0.01 % - 10 %) and frequency of 1 Hz. (B) Storage modulus of DTT/MMP crosslinked HA hydrogels as a function of frequency (1–10 Hz) and oscillation strain of 0.1 %. (C) Comparison of storage modulus of DTT/MMP crosslinked HA hydrogels prepared by varying ratios of DTT and MMP-cleavable peptide crosslinkers from the frequency sweep at an oscillation strain of 0.1 % and frequency of 1.6 Hz. $N \geq 3$ replicates per condition.

cancer [27–29] as well as other cancer cells [30–32]. However, the multiple crosslinking strategies employed to incorporate MMP-cleavable crosslinks also led to change in other hydrogel properties such as stiffness making it difficult to assess which specific property influences cancer cell behavior [27,28,30]. This underscores the need for decoupling of hydrogel properties to study MMP-mediated invasion of breast cancer cells *in vitro*. However, to the best of our knowledge, model systems that enable effective decoupling between hydrogel mechanical and structural properties such as modulus (stiffness) and mesh size while incorporating MMPs into the hydrogel matrix have not been reported.

To address this need, herein, we report structurally decoupled hyaluronic acid (HA)-based hydrogels as a 3D biomimetic platform to investigate the invasion of metastatic breast cancer cells mediated by MMPs. HA hydrogels were fabricated using varying ratios of biologically sensitive (i.e., MMP-cleavable peptide) and insensitive crosslinkers (i.e., Dithiothreitol (DTT) or polyethylene glycol dithiol (PEGDT)). Rheological measurements, swelling ratio analysis, estimated mesh size, permeability measurements, and degradation analysis were conducted to determine if HA hydrogels crosslinked with various ratios of DTT/MMP or PEGDT/MMP exhibited comparable mechanical and physical properties while exhibiting varying degradation profiles as a function of MMP-cleavable peptide concentration. Finally, we examined the impact of incorporated MMP-cleavable peptides on the invasion of MDA-MB-231Br metastatic breast cancer spheroids encapsulated in 3D HA hydrogels.

2. Materials and methods

2.1. Materials

Sodium Hyaluronate (Mw: 66–90 kDa, Part number: HA60K-5) was purchased from Lifecore Biomedical. Methacrylic anhydride, serum-free Dulbecco's Modified Eagle's Medium (DMEM), Poly (2-hydroxyethyl methacrylate) (p-HEMA), Dithiothreitol (DTT), Poly (ethylene glycol) dithiol (PEGDT), Dextran-fluorescein isothiocyanate (FITC-Dextran) with 20 kDa and 70 kDa molecular weights were purchased from Sigma Aldrich. Fetal bovine serum (FBS) was purchased from VWR Life Science. Penicillin-streptomycin (PS) was purchased from Gibco. Paraformaldehyde and Triton X were purchased from Alfa Aesar. AlexaFluor-488 labeled phalloidin and 4,6-diamidino-2-phenylindole (DAPI) was purchased from Invitrogen. The integrin binding peptide (RGD) with GCGYGRGDSPG sequence and MMP-cleavable peptide with CGPQGIWGQC sequence were purchased from GenScript. Collagenase type 2 was purchased from Worthington Biochemical Corporation.

2.2. Preparation of DTT-HA and PEGDT-HA hydrogels incorporating MMP-cleavable peptides

The synthesis of hyaluronic acid methacrylate (HAMA) was performed as described previously [16,33]. Briefly, an aqueous prepolymer solution containing 1 wt% of HA was prepared overnight. The HA solution was subjected to methacrylation through a reaction with ~18-fold molar excess of methacrylic anhydride at a temperature of 4 °C. The pH of the solution was meticulously maintained within the range of 8–10 by utilizing a 5 M NaOH solution. The synthesized HAMA was extracted

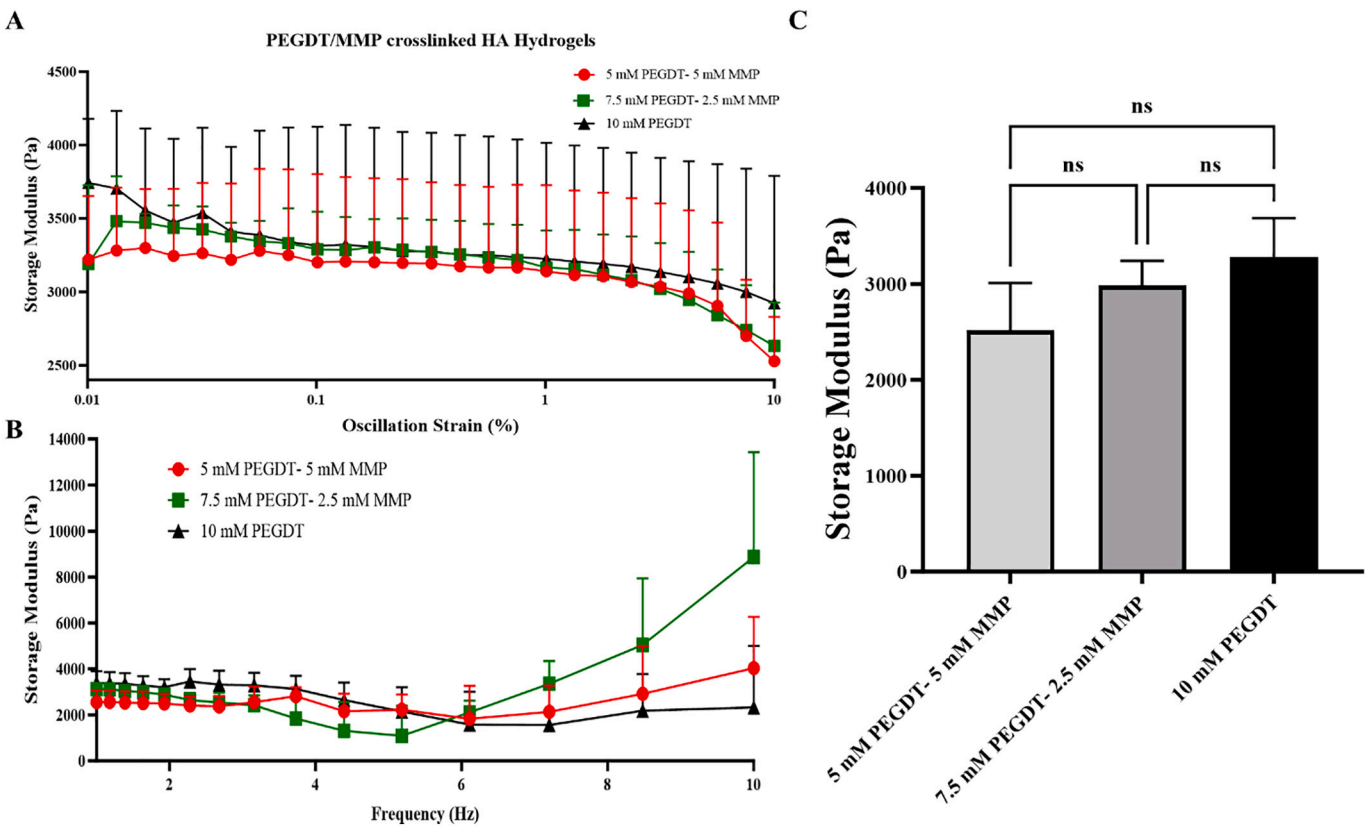

Fig. 2. Mechanical characterization of PEGDT/MMP crosslinked HA hydrogels. (A) Storage modulus of PEGDT/MMP crosslinked HA hydrogels as a function of oscillation strain (0.01 % - 10 %) and frequency of 1 Hz. (B) Storage modulus of PEGDT/MMP crosslinked HA hydrogels as a function of frequency (1–10 Hz) and oscillation strain of 0.1 %. (C) Comparison of storage modulus of PEGDT/MMP crosslinked HA hydrogels prepared by varying ratios of PEGDT and MMP-cleavable peptide crosslinkers from the frequency sweep at an oscillation strain of 0.1 % and frequency of 1.6 Hz. $N \geq 3$ replicates per condition.

by subjecting the final solution to a five-fold excess of cold acetone. The resulting mixture was then frozen and freeze-dried overnight. In the present study, HAMA with a methacrylation degree of ~125 % was employed, as determined by proton nuclear magnetic resonance (^{1}H NMR).

To fabricate DTT-HA and PEGDT-HA hydrogels, a gel precursor solution was formulated by incorporating 5 wt% HAMA into DMEM. The solution was incubated with the integrin binding peptide at a final concentration of 1 mg/mL overnight. The following day, DTT-HA hydrogels were prepared by incorporating various ratios of DTT and MMP-cleavable peptide crosslinkers into the hydrogel precursor solution. The total final concentration of crosslinkers was 10 mM, and different combinations of concentrations were used, including 10 mM DTT, 7.5 mM DTT with 2.5 mM MMP, and 5 mM DTT with 5 mM MMP. Similarly, to produce PEGDT-HA hydrogels, the precursor solution was combined with varying quantities of PEGDT and MMP concentrations to achieve a total crosslinker concentration of 10 mM. These included 10 mM of PEGDT, 7.5 mM of PEGDT with 2.5 mM of MMP, as well as 5 mM of PEGDT with 5 mM of MMP. The crosslinking process for HA hydrogels utilizes methacrylate groups on the HAMA backbone. The crosslinkers employed, including DTT, PEGDT, and MMP-cleavable peptides, all possess thiol groups at both ends. Gelation occurs through a thiol-Michael addition reaction between the methacrylated groups on the HAMA backbone and the thiol groups on the crosslinkers. This reaction forms covalent bonds resulting in a stable hydrogel network [15].

2.3. Mechanical characterization

Rheological evaluations were conducted utilizing an Anton Paar Modular Compact Rheometer (MCR) 302 using a previously established procedure [34]. The experiments were conducted using parallel plates positioned at a precisely controlled distance ranging from 2.5 to 3.0 mm. Prior to commencing the experiments, the hydrogel samples were immersed in phosphate-buffered saline (PBS) for two days. The swollen hydrogels were placed into the rheometer. Strain sweeps were conducted at a constant frequency of 1 Hz. These sweeps facilitated the determination of the storage modulus as a function of strain amplitude, aiding in the recognition of the linear viscoelastic region. The storage modulus of each hydrogel sample was subsequently determined using frequency sweep measurements conducted at a constant strain amplitude of 0.1 %.

2.4. Swelling ratio and mesh size estimation

To determine the equilibrium swollen weight of HA hydrogels, all synthesized hydrogels underwent lyophilization for 24 h. The lyophilized hydrogels were then weighed to obtain their resulting dry weights (Wd). The lyophilized hydrogels were then immersed in PBS for 48 h at 37 °C to achieve equilibrium swelling. Following this, the swollen samples were gently placed on a Kimwipe surface for 30 s to absorb any excess PBS. The swollen weight of the samples at this stage was recorded as Wi. The swelling ratio was calculated by dividing the mass of water absorbed by the mass of the dry sample (Wd) [35].

$$\text{Swelling Ratio } Q = [(Wi - Wd)/Wd] \times 100$$

The evaluation of mesh size was performed following the methodology established by Canal and Peppas, a well-recognized technique in the characterization of hydrogels [36]. This approach focuses on determining the molecular weight between crosslinks (M_c) by utilizing the equilibrium swelling ratio (Q), a fundamental parameter described

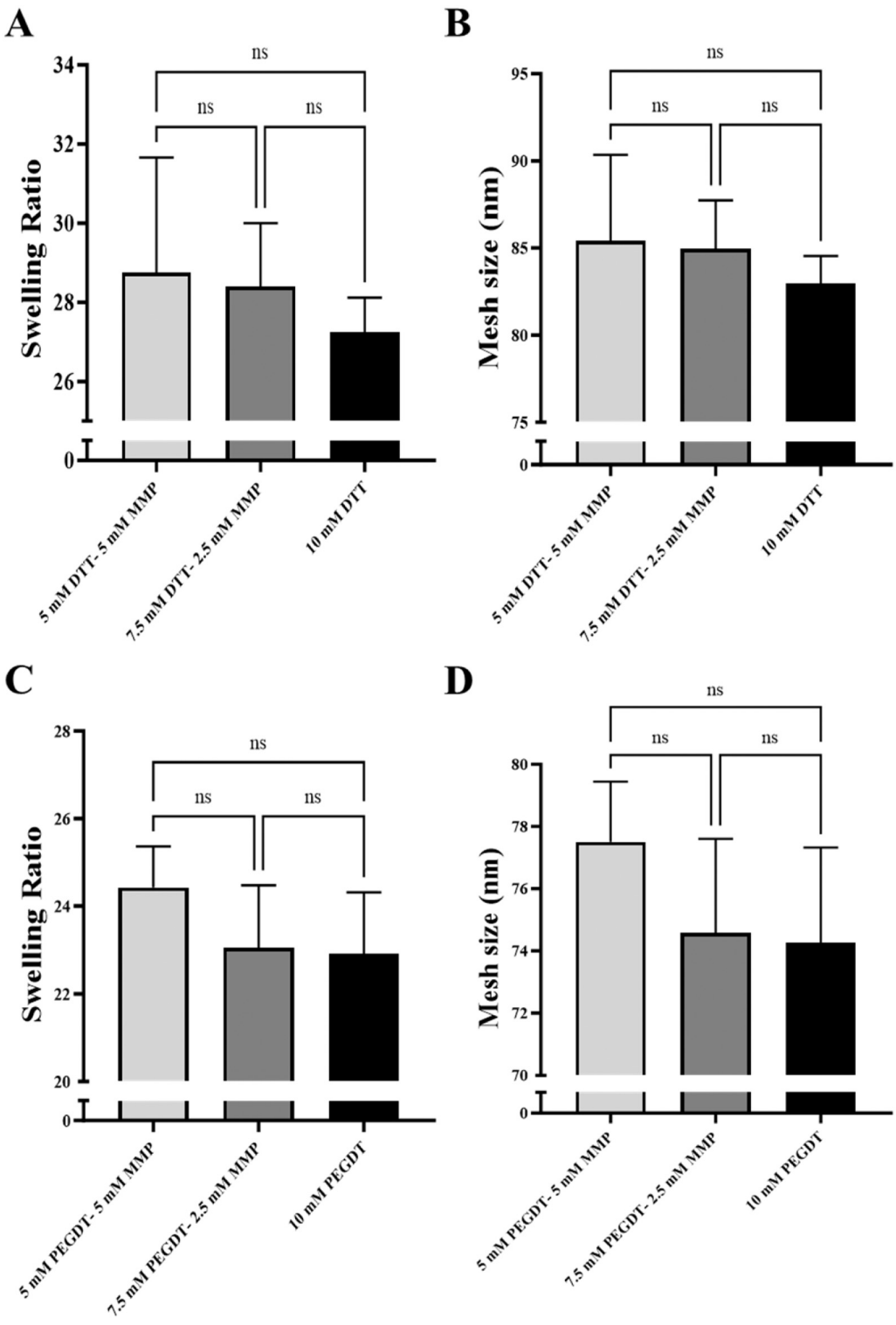

Fig. 3. Swelling ratio and estimated mesh size of DTT/MMP and PEGDT/MMP crosslinked HA hydrogels. (A, B) Swelling ratio and mesh size of DTT/MMP crosslinked HA hydrogels prepared by varying ratio of DTT and MMP-cleavable peptide crosslinkers (C, D) Swelling ratio and mesh size of PEGDT/MMP crosslinked HA hydrogels prepared by varying ratio of PEGDT and MMP-cleavable peptide crosslinkers. $N \geq 7$ replicates per condition.

in the Flory-Rehner Eq. [37]. It was assumed that the physical characteristics of HAMA used in this study would be similar to those of unmodified HA. The M_c value plays a crucial role in determining the mean square end-to-end distance of the chain in the absence of the solvent. By using established methodologies in polymer network analysis, the mesh size was computed based on the theoretical mesh size calculation [38].

2.5. Scanning electron microscopy (SEM) and morphological analysis

To examine the microstructural architecture of HA hydrogels crosslinked with DTT/MMP or PEGDT/MMP crosslinkers, we utilized scanning electron microscopy (SEM). After fabricating the HA hydrogels, the samples were frozen in liquid nitrogen and then lyophilized overnight. For cross-sectional views, the lyophilized hydrogels were cut through

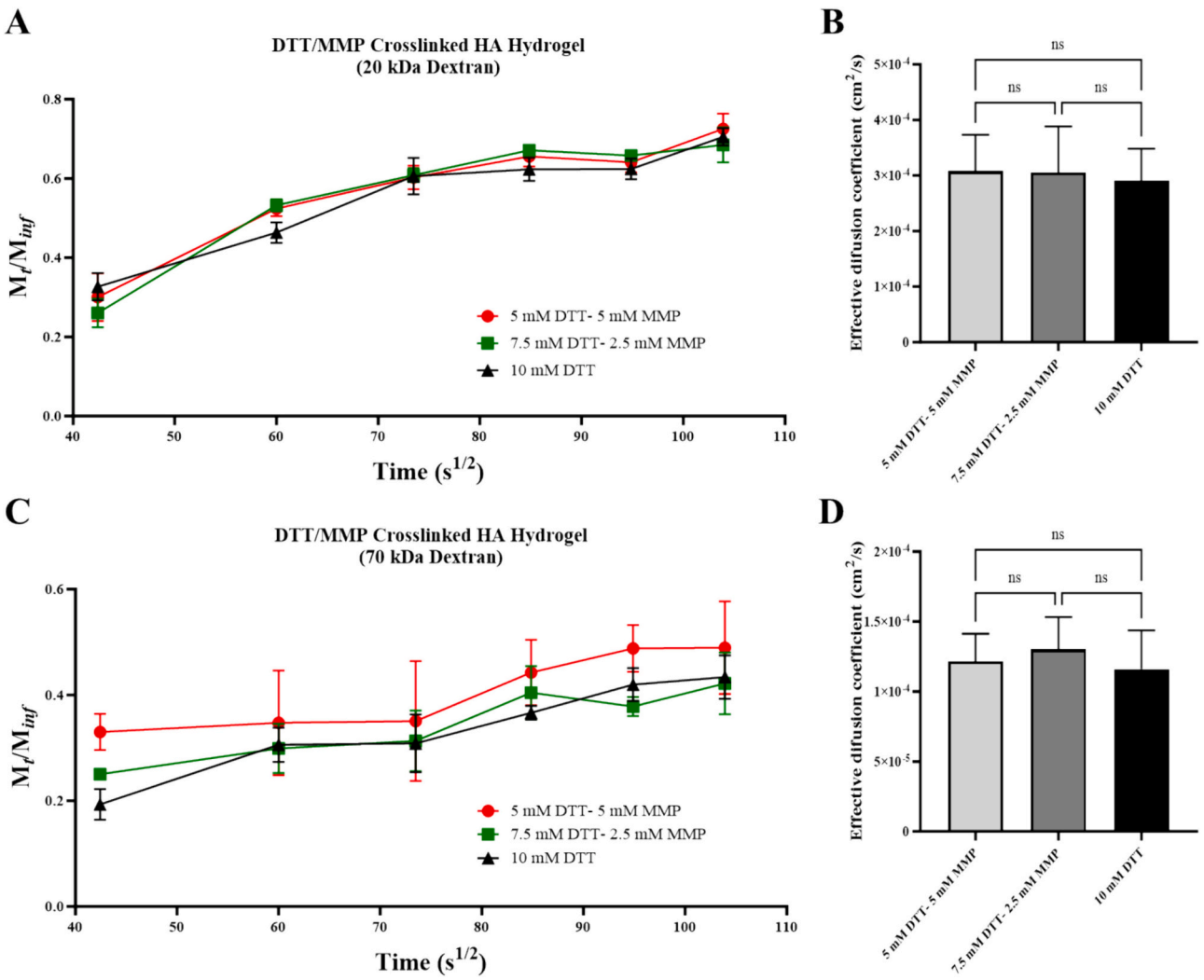

Fig. 4. Permeability and effective diffusion coefficient of DTT/MMP crosslinked HA hydrogels utilizing dextran molecules with molecular weights of 20 kDa and 70 kDa. (A, C) The released fraction (M_t/M_{inf}) of 20 kDa and 70 kDa dextran from DTT/MMP crosslinked HA hydrogels over time respectively. (B, D) Effective diffusion coefficients (cm^2/s) of 20 kDa and 70 kDa dextrans through DTT/MMP crosslinked HA hydrogels. $N \geq 5$ replicates per condition.

the middle, while uncut samples were used for top-view analysis. The prepared samples were then sputter-coated with gold using a Hummer® 6.6 Sputter Coater. SEM analysis was performed with an SU3500 Scanning Electron Microscope at an accelerating voltage of 5.00 kV to capture images of the hydrogel structure as described previously [34].

2.6. Permeability measurements

To evaluate the diffusivity of HA hydrogels, we employed a well-established method [39]. Briefly, HA hydrogels were exposed to a solution containing FITC-Dextran molecules at a concentration of 1 mg/mL. We employed FITC-Dextran with a molecular weight of 20 kDa and 70 kDa and these were dissolved in PBS (pH = 7). Incubation occurred for a duration of 3 days at a controlled temperature of 37 °C. Following this incubation period, the hydrogels were submerged in 1 mL of PBS, and at regular intervals of 30 min, 100 μL samples were drawn over a total period of 3 h. An additional sample was collected after 24 h. Fluorescence intensity measurements were conducted using the FilterMax F5 multi-mode microplate reader. These readings were then utilized to determine the concentration of released FITC-Dextran from the HA hydrogels. The correlation between the fluorescence readings and known concentrations established through a standard curve allowed for the quantification of the released FITC-Dextran concentrations by using the below formula [39].

$$\frac{M_t}{M_\infty} = 2\left[\frac{D_e t}{\pi x^2}\right]^{\frac{1}{2}}$$

The calculation of effective diffusion coefficient (D_e) utilized Fick's law of diffusion. In this context, M_t represents the released mass of FITC-Dextran at a given time t, M_∞ denotes the total released mass of FITC-Dextran from the hydrogel in the solution, D_e is the diffusion coefficient, t stands for time, and x refers to the hydrogel depth, following methodologies previously described [40].

2.7. Degradation analysis

Degradation analysis was conducted to quantitatively assess the rate of degradation of HA hydrogels by the collagenase type II enzyme that was acquired in a powdered form with a solid concentration of 255 U/mg. Initially, each fabricated hydrogel was immersed in PBS for a duration of 2 days to attain a state of equilibrium swelling. The weights of all HA hydrogels were measured after their placement on a Kimwipe for the purpose of eliminating any surplus PBS. The HA hydrogels were then fully immersed in a solution containing collagenase type II enzyme at a concentration of 50 U/mL in PBS, a value chosen based on the effective range reported in the literature [41,42]. Prior to weighing the

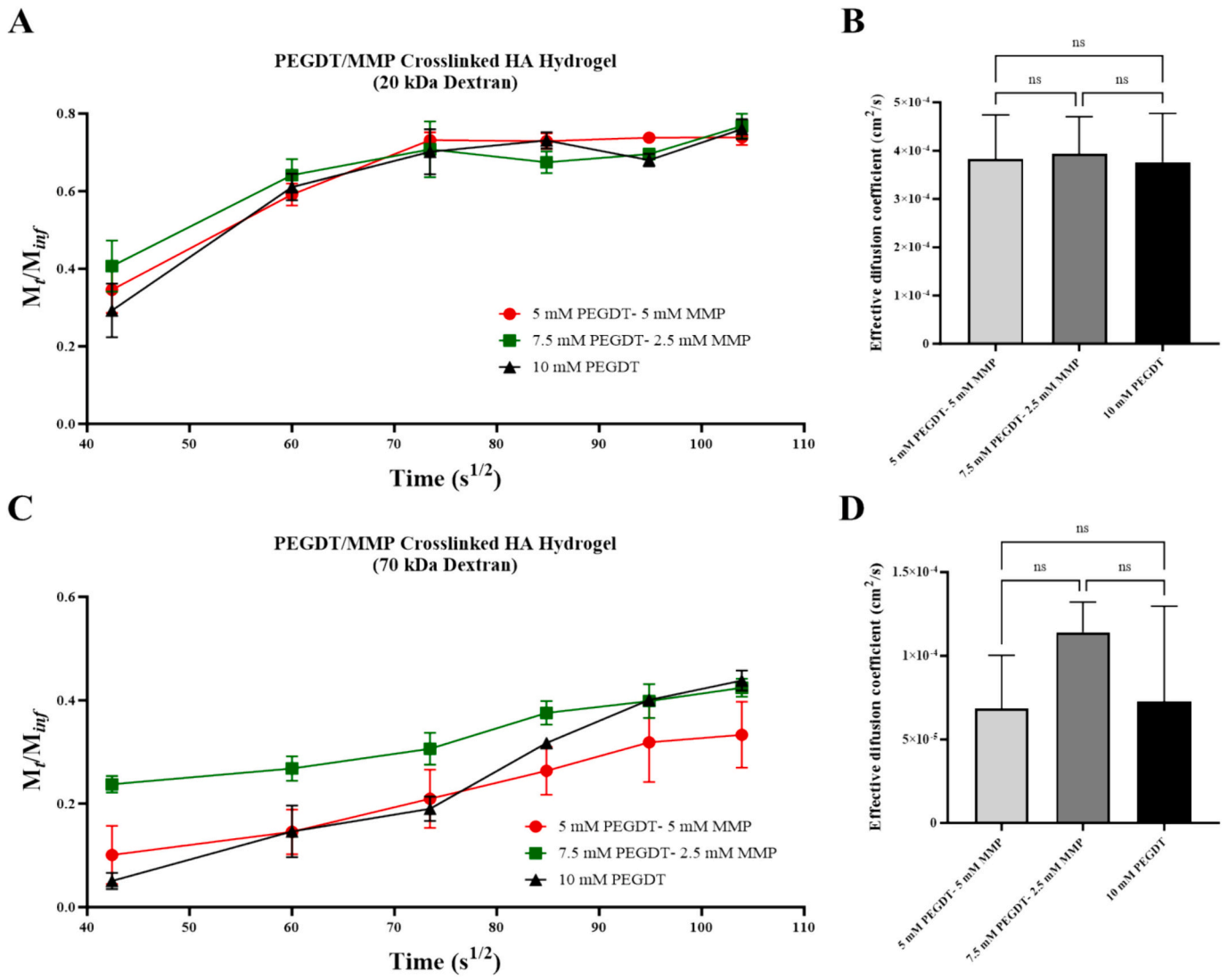

Fig. 5. Permeability and effective diffusion coefficients of PEGDT/MMP crosslinked HA hydrogels utilizing dextran molecules with molecular weights of 20 kDa and 70 kDa. (A, C) The released fraction (M_t/M_{inf}) of 20 kDa and 70 kDa dextran from PEGDT/MMP crosslinked HA hydrogels over time respectively. (B, D) Effective diffusion coefficients (cm^2/s) of 20 kDa and 70 kDa dextrans through PEGDT/MMP crosslinked HA hydrogels. $N \geq 5$ replicates per condition.

samples, any excess collagenase type II solution was removed via placement on a Kimwipe. Subsequently, the weights of each hydrogel were measured at various time intervals over a 4 h time period, while ensuring that the hydrogels were placed in the incubator during periods when weight measurements were not being conducted [43].

2.8. Cell culture

In this study, we utilized the MDA-MB-231Br cell line, a brain metastatic derivative of the MDA-MB-231 triple-negative breast cancer cell line. These cells were cultured using established protocols [16,44]. In particular, the cells were cultured in Dulbecco's Modified Eagle Medium (DMEM) high glucose, supplemented with 10 % FBS and 1 % PS, at a controlled temperature of 37 °C and 5 % CO_2. The cells were passaged when they reached approximately 80 % confluency and were subsequently utilized in making cell spheroids. Cells with <25 passages were utilized in all studies.

2.9. Tumor cell spheroid construction

Cell spheroids were prepared using a well-established method [45–47]. Briefly, a 20 mg/mL solution of p-HEMA was prepared in 95 % ethanol. To achieve a non-cell adhesive surface, each well of a 96-well conical bottom plate was coated with approximately 30 μL of the p-HEMA solution. The plate was then dried in a laminar hood overnight. To form MDA-MB-231Br cell spheroids, cell dilutions were prepared at a concentration of 10,000 cells per 100 μL. The cell suspensions were carefully placed into the pre-coated wells of a 96-well conical bottom plate. Subsequently, the plate was centrifuged at 1000*g* for 10 min to facilitate the formation of cell spheroids. Post-centrifugation, 2.5 μL of growth factor reduced Matrigel was added to the wells and the plate was then incubated overnight.

2.10. Spheroid encapsulation, optical imaging, and cell spheroid area measurements

To encapsulate spheroids in HA hydrogels, the gel precursor solution with the desired ratio of crosslinkers at a final concentration of 10 mM was prepared and then 100 μL of this solution was added to each well of a 96-well plate. Next, retrieved cell spheroids (one spheroid per gel) were immediately embedded in the gel precursor solution and spheroid-laden hydrogels were formed in ~2 h following which cell culture media was added on top of the hydrogels. The spheroid-laden hydrogels were cultured for 14 days. Throughout this period, the culture media

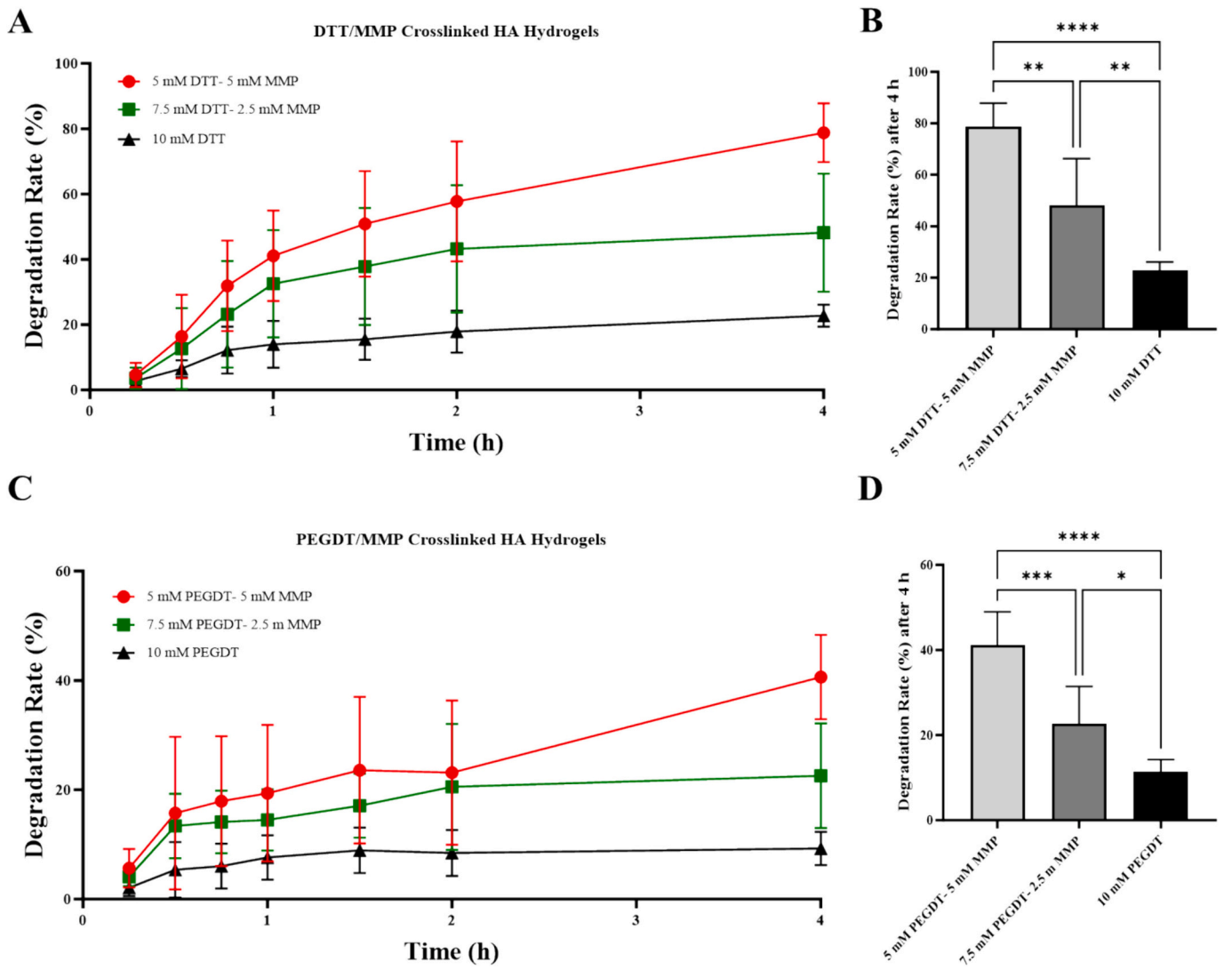

Fig. 6. Degradation analysis of DTT/MMP and PEGDT/MMP crosslinked HA hydrogels using Collagenase type II enzyme. (A, C) Degradation rate profiles of DTT/MMP and PEGDT/MMP crosslinked HA hydrogels in the enzyme environment over time. (B, D) Degradation rate of DTT/MMP and PEGDT/MMP crosslinked HA hydrogels after immersing for 4 h in enzyme solution with 50 U/mL concentration. $N = 6$ replicates per condition. Statistically significant difference indicator via one-way ANOVA followed by Tukey-HSD test: (*, $p < 0.05$) (**, $p < 0.01$) (***, $p < 0.001$) (****, $p < 0.0001$).

underwent replacement every 4 days. Brightfield images for day 0 were taken ~2h after encapsulation. The area of cell spheroids was assessed using Image-J software on days 0 and 14, considering both the cross-sectional area of the spheroid and the spread area of cells that migrated from the spheroids, as previously described [45,48]. Briefly, the boundaries of the cell spheroids were manually delineated. In cases where cell migration from the spheroids was detected, these migrating boundaries were also included in the calculation of the spheroid areas. The area ratio was calculated by dividing the total area of the encapsulated spheroid and spread area at day 14 by the encapsulated spheroid area at day 0.

2.11. F-actin staining

To observe the F-actin filaments in the MDA-MB-231Br cell spheroids encapsulated in HA hydrogels, we performed staining for F-Actin using a previously utilized protocol [14]. In brief, the encapsulated spheroids were fixed using 4 % paraformaldehyde for 1 h, followed by permeabilization with a 0.25 % Triton X solution in PBS for another hour. Subsequently, the spheroids were blocked for 1 h using a 5 % FBS solution in PBS. Subsequently, AlexaFluor-488 labeled phalloidin (Invitrogen) [1:500] was utilized for staining the actin filaments within the cells. For visualizing the cell nuclei, DAPI staining [1:1000] was performed. Fluorescence microscopy was performed using an Olympus IX83 microscope with a spinning disc confocal attachment.

2.12. Statistical analysis

Aside from mechanical characterization, which included a minimum of three samples per condition, all other characterizations were conducted in two distinct experimental trials, with each condition tested in at least two replicates. Unless explicitly stated, all numerical values are reported as the mean ± standard deviation. Statistical analyses were performed using the PRISM software package. For comparison between samples, one-way analysis of variance (ANOVA) was performed. Following ANOVA, post-hoc comparisons were performed utilizing the Tukey-Honest Significant Difference (Tukey-HSD) test. A p-value of <0.05 was considered to be statistically significant.

3. Results and discussion

In this study, we present a HA hydrogel-based 3D biomimetic

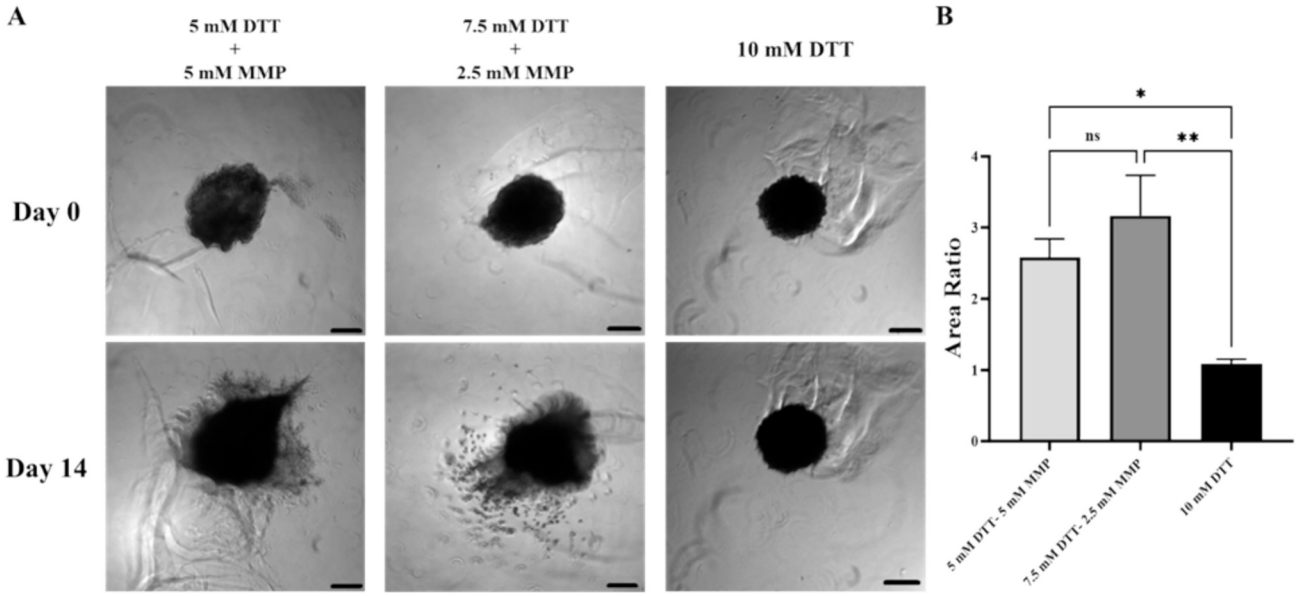

Fig. 7. Invasion of encapsulated MDA-MB-231Br cell spheroid in DTT/MMP crosslinked HA hydrogels. (A) Representative bright field images of encapsulated cell spheroid at day 0 and day 14 post encapsulation. (B) Ratio of the area of encapsulated spheroid in DTT/MMP crosslinked HA hydrogels on day 14 compared to day 0. Scale bar = 200 μm. $N \geq 5$ replicates per condition. Statistically significant difference indicator via one-way ANOVA followed by Tukey-HSD test: (*, $p < 0.05$) (**, $p < 0.01$).

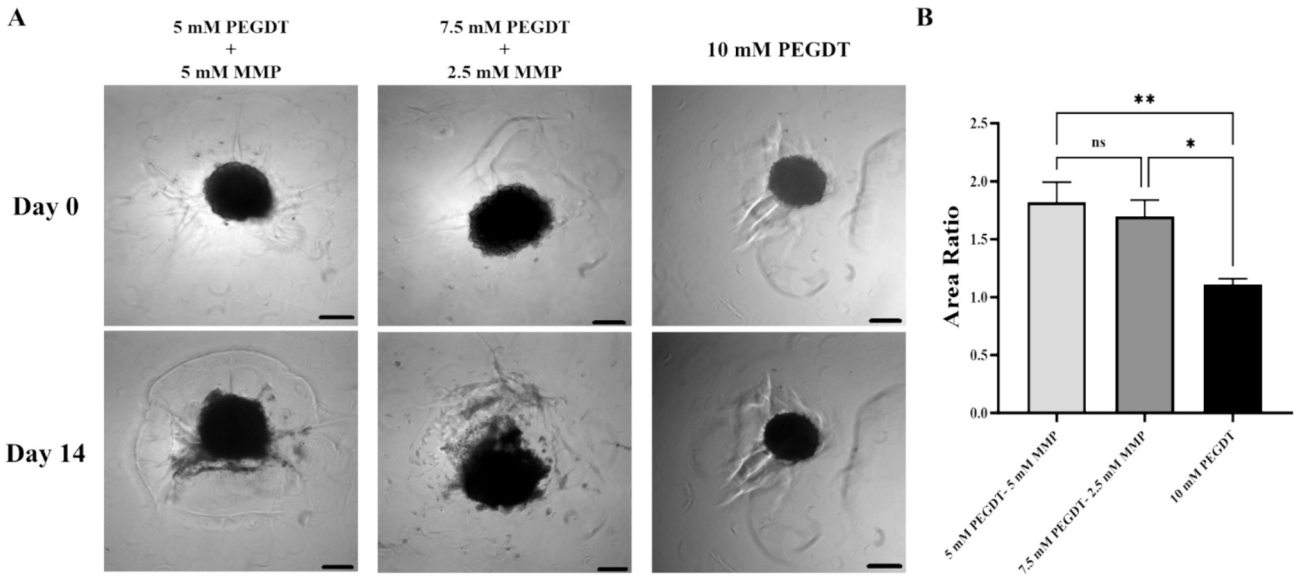

Fig. 8. Invasion of encapsulated MDA-MB-231Br cell spheroid in PEGDT/MMP crosslinked HA hydrogels. (A) Representative bright field images of encapsulated cell spheroid at day 0 and day 14 post encapsulation. (B) Ratio of the area of encapsulated spheroid in PEGDT/MMP crosslinked HA hydrogels on day 14 compared to day 0. Scale bar = 200 μm. $N \geq 5$ replicates per condition. Statistically significant difference indicator via one-way ANOVA followed by Tukey-HSD test: (*, $p < 0.05$) (**, $p < 0.01$).

platform that allows decoupling between hydrogel mechanical and structural properties such as modulus (stiffness) and mesh size while incorporating MMPs into the hydrogel matrix to study the invasion of metastatic breast cancer spheroids *in vitro*. While the influence of MMP-cleavable peptides on cancer cell response has been studied in conjunction with other cues [27,30], the specific impact of degradable cues on cancer cell invasion, especially, in the context of brain metastatic breast cancer remains unexplored. Herein, for the first time, we have employed structurally decoupled HA-based hydrogels crosslinked with varying ratios of biologically sensitive to insensitive crosslinkers to investigate the impact of MMP-cleavable peptides on the invasion of encapsulated MDA-MB-231Br brain metastatic breast cancer cell spheroids. A key feature of this approach is that both biologically sensitive (i.e., MMP) and insensitive (i.e., DTT or PEGDT) crosslinkers are thiol terminated on both ends enabling HAMA crosslinking via the Michael-type addition reaction.

3.1. Mechanical characterization

To determine if utilizing varying ratios of DTT or PEGDT with MMP-cleavable peptide crosslinkers impact mechanical properties of the resulting HA hydrogels, rheological analysis was conducted. The storage modulus for each hydrogel condition was obtained by conducting a sweep over a range of oscillation strains at a constant frequency of 1 Hz

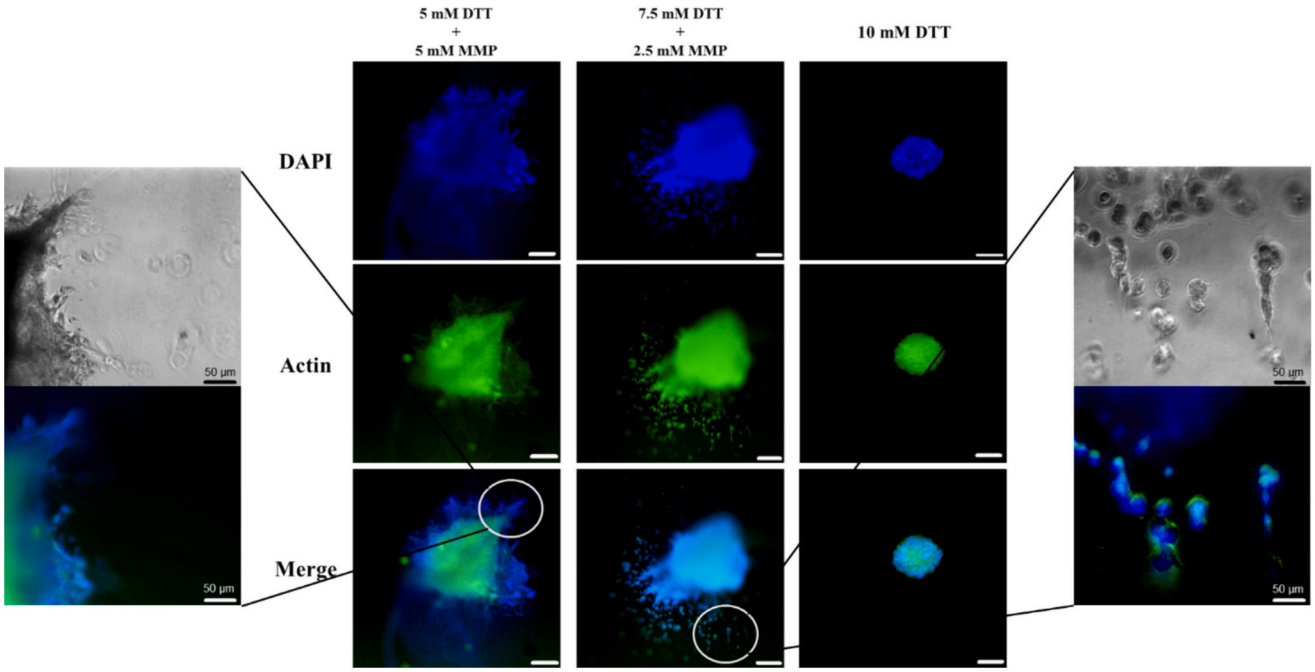

Fig. 9. F-actin staining of 10 k MDA-MB-231Br cell spheroid encapsulated in DTT/MMP crosslinked HA hydrogels on day 14. Green = F-actin, Blue = DAPI, Scale bar = 200 μm. (For interpretation of the references to colour in this figure legend, the reader is referred to the web version of this article.)

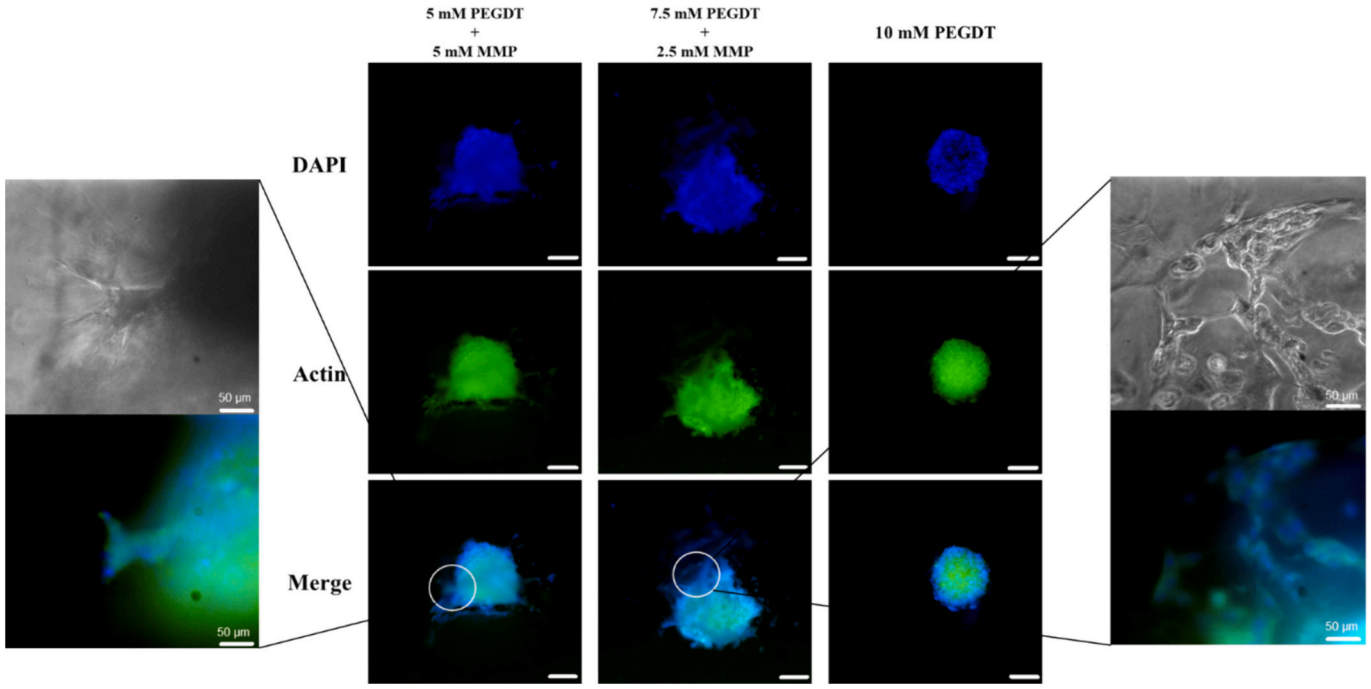

Fig. 10. F-actin staining of 10 k MDA-MB-231Br cell spheroid encapsulated in PEGDT/MMP crosslinked HA hydrogels on day 14. Green = F-actin, Blue = DAPI, Scale bar = 200 μm. (For interpretation of the references to colour in this figure legend, the reader is referred to the web version of this article.)

(Fig. 1A, 2A). Next, a frequency sweep was performed over a range of 1–10 Hz at constant strain amplitude of 0.1 % (Fig. 1B, 2B). The results of the frequency sweep analysis at constant strain amplitude showed that storage modulus of HA hydrogels crosslinked with varying ratios of DTT/MMP or PEGDT/MMP in the range of 1–2 Hz at 0.1 % oscillation strain were in the linear viscoelastic region. Thus, the storage modulus data used to compare the mechanical properties of each hydrogel condition were determined at 0.1 % oscillation strain and 1.6 Hz.

As shown in Fig. 1C and Fig. 2C, the results revealed that there was no significant difference in the storage modulus of DTT/MMP or PEGDT/MMP crosslinked HA hydrogels. Specifically, the storage modulus values were measured as 1121 ± 331.9 Pa, 850.2 ± 85.2 Pa, and 921.0 ± 195.8 Pa for the hydrogels crosslinked with 5 mM of DTT and 5 mM of MMP, 7.5 mM of DTT and 2.5 mM of MMP, and 10 mM of DTT, respectively. Similarly, the storage modulus of HA hydrogels crosslinked with 5 mM of PEGDT and 5 mM of MMP was 2517 ± 491.5 Pa. The hydrogels crosslinked with 7.5 mM of PEGDT and 2.5 mM of MMP had a storage modulus of 2986 ± 254.1 Pa. Finally, the hydrogels

crosslinked with 10 mM of PEGDT had a storage modulus of 3280 ± 406.6 Pa. The findings revealed that the partial replacement of biologically inactive crosslinkers with MMP-cleavable peptide crosslinkers for the fabrication of HA hydrogels did not have a substantial impact on the storage modulus of the hydrogels. Thus, hydrogels with different combinations of sensitive and non-sensitive crosslinkers in each condition (i.e., DTT or PEGDT) exhibited similar mechanical properties.

3.2. Swelling ratio and estimated mesh size

The hydrogel's swelling ratio and mesh size play a crucial role in determining the physical microenvironment that cancer cells experience, ultimately influencing the way they respond to biochemical and biophysical signals [28]. Moreover, the hydrogel's mesh size, which represents the average distance between crosslinks in the polymer network, plays an important role in determining molecule diffusion and the physical confinement of cells in the hydrogel matrix. The significance of these physical microenvironmental cues is highlighted by their ability to regulate the availability and transport of nutrients and oxygen, growth factors, and signaling molecules within the hydrogel [49]. This directly affects the behavior of cells, including cell morphology and migration [50].

Results of swelling ratio measurements demonstrated that there were no significant differences observed in the swelling ratio of DTT and DTT/MMP crosslinked HA hydrogels across all conditions. In particular, the swelling ratio for the hydrogels crosslinked with 5 mM of DTT and 5 mM of MMP, 7.5 mM of DTT and 2.5 mM of MMP, and 10 mM of DTT were 28.8 ± 2.9, 28.4 ± 1.6, and 27.3 ± 0.9, respectively. Further, the calculated theoretical mesh sizes were 85.4 ± 4.9 nm, 84.9 ± 2.8 nm, and 83 ± 1.6 nm for hydrogels crosslinked with 5 mM of DTT and 5 mM of MMP, 7.5 mM of DTT and 2.5 mM of MMP, and 10 mM of DTT, respectively (Fig. 3A, B).

Similarly, the results from swelling ratio measurements and calculated theoretical mesh sizes indicate that PEGDT and PEGDT/MMP crosslinked HA hydrogels also had statistically similar swelling ratios and mesh sizes. In particular, the swelling ratios were 24.4 ± 0.9, 23.1 ± 1.4, and 22.9 ± 1.4 and the theoretical mesh sizes were 77.5 ± 1.9 nm, 74.6 ± 3 nm, and 74.3 ± 3.1 nm for hydrogels crosslinked with 5 mM of PEGDT and 5 mM of MMP, 7.5 mM of PEGDT and 2.5 mM of MMP, and 10 mM of PEGDT, respectively (Fig. 3C, D). Based on the theory of rubber elasticity, materials generally exhibit a decrease in swelling ratio as the crosslinking density increases or the average molecular weight between the cross-links decreases [51,52]. Therefore, the absence of significant differences in swelling ratios and calculated mesh sizes among all PEGDT/MMP crosslinked HA hydrogels is indicative of the structural similarity of these hydrogels. We also performed SEM to assess the microstructural architecture of the hydrogels. The surface and cross-sectional morphologies of HA hydrogels crosslinked with DTT/MMP (Fig. S1) and PEGDT/MMP (Fig. S2) were similar and consistent within their groups further confirming the structural similarity of these hydrogels.

3.3. Permeability

To determine if utilizing varying ratios of DTT/MMP-cleavable peptide crosslinkers impact permeability of the resulting HA hydrogels, we measured permeability through fluorescent dextran release studies of two different molecular weights (i.e., 20 kDa and 70 kDa).

We quantified the concentration ratio of released dextran at a specific time (M_t) to the total concentration released at infinite time (24 h) (M_{inf}) for HA hydrogels crosslinked with DTT/MMP by utilizing a standard curve generated using fluorescently labeled dextrans (Fig. S3 and Fig. S4). This ratio is graphed against the square root of time ($s^{1/2}$) and the slope of this graph provides the effective diffusion coefficient of dextran molecules with varying molecular weights from DTT/MMP crosslinked HA hydrogels [39]. The calculated effective diffusion coefficients for DTT/MMP crosslinked HA hydrogels revealed no significant difference in permeability between the hydrogels for both sizes of dextran molecules (Fig. 4B, D).

Similarly, the release ratio of dextran at a specific time compared to its complete release after 24 h in HA hydrogels crosslinked with PEGDT/MMP, was determined through the same calibration curve of fluorescently labeled dextran (Fig. S3 and Fig. S4). The effective diffusion coefficients calculated for PEGDT/MMP crosslinked HA hydrogels indicate consistent permeability levels across the hydrogels, regardless of the size of dextran molecules (Fig. 5B, D). These results further demonstrate that the average mesh size of PEGDT/MMP crosslinked hydrogels is similar. This is supported by the fact that the hydrogels did not exhibit any significant difference in diffusion rate or effective diffusion coefficients when evaluating their permeability to dextran molecules of varying molecular weights and, consequently, different hydrodynamic radius.

3.4. Degradation analysis

Through mechanical characterization, swelling measurements, mesh size estimation, SEM, and permeability measurements, we determined that utilizing varying ratios of DTT (or PEGDT)/MMP cleavable peptide crosslinkers has minimal impact on the resultant hydrogel properties. However, the inclusion of MMP-cleavable peptide crosslinkers should enable cell mediated matrix degradation via MMPs. Therefore, we first sought to test if utilizing varying ratios of DTT/MMP-cleavable peptide crosslinkers influences degradation behavior of the resulting HA hydrogels.

Fig. 6A illustrates the timeline of degradation for DTT/MMP crosslinked HA hydrogels. The degradation rate of the hydrogel by collegenase type II enzyme increased as the ratio of MMP-cleavable peptide in the hydrogel network increased. This data demonstrates that the presence of a MMP-cleavable peptide as a crosslinker leads to a considerably higher degree of degradation, even within a brief timeframe, as depicted in Fig. 6B. Specifically, the degradation percentages of hydrogels crosslinked with different concentrations of DTT and MMP after 4 h were as follows: 78.8 ± 9.0 % for 5 mM of DTT and 5 mM of MMP, 48.2 ± 18.1 % for 7.5 mM of DTT and 2.5 mM of MMP, and 22.8 ± 3.4 % for 10 mM of DTT.

Similar results were also noted in the PEGDT/MMP crosslinked HA hydrogel system. Fig. 6C demonstrates the timeline of degradation for HA hydrogels crosslinked with PEGDT/MMP. Rapid degradation rate was observed by an increase in the ratio of MMP-cleavable peptide crosslinker in HA hydrogels crosslinked with PEGDT/MMP. This data also reveals that the inclusion of an MMP-cleavable peptide as a crosslinker results in a significantly greater degree of degradation, even within a short timescale, as seen in Fig. 6D. Specifically, the percentage of hydrogel degradation for hydrogels crosslinked with 5 mM of PEGDT and 5 mM of MMP, 7.5 mM of PEGDT and 2.5 mM of MMP, and 10 mM of PEGDT were found to be 41.2 ± 7.8 %, 22.7 ± 8.8 %, and 11.4 ± 2.8 %, respectively. The analysis of the enzymatic degradation profiles of DTT/MMP and PEGDT/MMP crosslinked HA hydrogels shows that the presence of MMP-cleavable peptide crosslinker that is sensitive to biological degradation significantly accelerates the degradation of hydrogels. This is supported by the observed higher degradation rates when there is a higher concentration of MMP-cleavable peptide in the hydrogel network. The results of our degradation analysis align with previous studies that utilized MMP-cleavable peptides in hydrogel networks to create bioactive polymeric systems [53,54].

3.5. MDA-MB-231Br cell spheroid invasion study

Prior studies have shown that hydrogel biophysical cues, such as matrix stiffness [14], crosslink density [27], and structure of the network [55], can influence cancer cell response. Herein, DTT/MMP or PEGDT/MMP crosslinked HA hydrogels exhibited comparable

characteristics, as indicated by measurements of mechanical and physical properties, however, the degradation profiles varied as a function of MMP-cleavable peptide crosslinker concentration. Thus, these hydrogels enabled us to investigate the impact of cell-mediated matrix degradation on the invasion of brain metastatic breast cancer cell spheroids *in vitro*.

We encapsulated 10 k MDA-MB-231Br cell spheroid in DTT/MMP or PEGDT/MMP crosslinked HA hydrogels to study invasion over a period of 14 days. The cross-sectional area measurements at day 14 vs. day 0 revealed cellular invasion within the HA hydrogel network with MMP sensitivity. Although there were no differences in the measured cross-sectional area between the conditions of MMP-sensitive HA hydrogels crosslinked with 5 mM of DTT and 5 mM of MMP, and 7.5 mM of DTT and 2.5 mM of MMP, both conditions exhibited a significant difference compared to non-sensitive HA hydrogels crosslinked with 10 mM of DTT (Fig. 7). In particular, the ratio of cell-covered cross-sectional area measured on day 14 to day 0 was 2.6 ± 0.6, 3.2 ± 1.3, and 1.1 ± 0.2 respectively, for the highest to lowest ratio of the MMP-cleavable peptide crosslinker in the case of DTT/MMP crosslinked HA hydrogels. These results also suggest that even lower concentrations of MMP-cleavable peptides (i.e., 2.5 mM of MMP) were sufficient to support cancer cell invasion *in vitro*.

Similar results was observed in the case of PEGDT/MMP crosslinked HA hydrogels. Hydrogels incorporating MMP-cleavable peptides showed significantly greater 3D cell invasion compared to those without MMP-cleavable peptides as determined using cross-sectional area measurements (Fig. 8). Specifically, the cross-sectional area ratio for hydrogels crosslinked with 5 mM of PEGDT and 5 mM of MMP, 7.5 mM of PEGDT and 2.5 mM of MMP, and 10 mM of PEGDT were found to be 1.8 ± 0.4, 1.7 ± 0.3, and 1.1 ± 0.1 respectively. The comparable crosslinking density, pore size, and RGD ligand density in both DTT/MMP and PEGDT/MMP crosslinked HA hydrogels indicate that cellular invasion is mainly regulated by the degradability of the hydrogel through MMP-mediated processes.

The cell cytoskeleton regulates various physiological cell processes, and actin, as one of constituent of the cytoskeleton, provides significant control over many of these cellular processes such as cell movement [56,57]. Specifically, within cancer cells, the polymerization of F-actin in the cytoskeleton correlates with the enhancement of properties like migration, invasiveness, and metastasis [58,59]. F-actin staining revealed invaded cells with well-developed actin cytoskeleton at the periphery of spheroids within both DTT/MMP and PEGDT/MMP crosslinked HA hydrogel structures containing MMP-cleavable sites. Moreover, F-actin staining showed the presence of invasive protrusions along the spheroid outer edge in HA hydrogels with MMP-cleavable peptide crosslinkers (Figs. 9, 10). Conversely, the cell spheroid encapsulated in HA hydrogels crosslinked with 10 mM of DTT or PEGDT exhibited round morphology with ill-formed F-actin fibers and no invasive protrusions along their periphery (Figs. 9, 10). This suggests that the lack of degradable sites in these hydrogels prevents F-actin remodeling, which is required for cancer cell invasion.

Overall, our results demonstrate the utility of these structurally decoupled HA hydrogels that exhibit similar mechanical and physical properties while providing varying degradation cues to study metastatic breast cancer invasion and the associated mechanisms *in vitro*. This can lead to a better understanding of the invasion process and the identification of novel therapeutic targets. This, in turn, could enable therapeutic approaches to inhibit the invasion of metastatic breast cancer cells in the long term. In addition, these hydrogels can be utilized to screen potential anti-invasive drugs by providing a controlled environment that mimics the tumor microenvironment. However, we note the following limitations of the work: (1) This study employed a brain metastatic breast cancer cell line (MDA-MB-231Br) to study invasion. Future research could test additional cell types such as non-invasive cancer cells and patient-derived cancer cells, to enhance our understanding of tumor heterogeneity and the mechanisms of invasion across different cancer types. (2) Future studies could utilize photo-crosslinkers to form HA hydrogels and determine if decoupling can be achieved in these hydrogel systems. (3) Future research could explore how varying the total concentration and ratios of biologically sensitive and insensitive crosslinkers impacts hydrogel stiffness and biodegradability, and subsequently cancer cell invasion. (4) This study did not examine other potential factors in the tumor microenvironment, such as growth factors and cytokines, which can also influence invasion. Future research could investigate these factors and how they influence invasion in the hydrogel environment.

4. Conclusions

In this study, we developed structurally decoupled HA hydrogels as a 3D biomimetic model to study MMP-mediated invasion in brain metastatic breast cancer cell spheroids *in vitro*. To form structurally decoupled HA hydrogels, we employed different ratios of MMP-sensitive (i.e., MMP-cleavable peptide) and insensitive crosslinkers (i.e., DTT or PEGDT), and found that there was no significant difference in the storage modulus, swelling ratio, mesh size, or permeability of the resulting HA hydrogels. However, varying the MMP-cleavable peptide ratios significantly influenced the degradation rates of the hydrogel in the presence of collagenase type II enzyme. Accordingly, hydrogels incorporating MMP-cleavable peptides also supported invasion of encapsulated MDA-MB-231Br cell spheroids cultured over a period of 14 days. Furthermore, F-actin staining revealed that invaded cells formed a well-organized actin cytoskeleton at the spheroid periphery in hydrogels incorporating MMP-cleavable peptides as opposed to those without MMP-cleavable peptides. In sum, our findings demonstrate that structurally decoupled HA hydrogels could be used as a 3D platform for studying MMP-mediated metastatic breast cancer cell invasion *in vitro*.

CRediT authorship contribution statement

Kasra Goodarzi: Writing – review & editing, Writing – original draft, Visualization, Validation, Methodology, Investigation, Formal analysis, Data curation, Conceptualization. **Shreyas S. Rao:** Writing – review & editing, Supervision, Resources, Project administration, Methodology, Investigation, Funding acquisition, Conceptualization.

Declaration of competing interest

The authors declare that they have no conflicts of interest.

Data availability

Data will be made available on request.

Acknowledgements

This work was supported, in part, by the National Science Foundation (CBET 1749837, to S.R.). We also acknowledge financial support from the Alabama Graduate Research Scholars Program (GRSP) funded through the Alabama Commission for Higher Education and administered by the Alabama EPSCoR (to K.G.). The authors thank Dr. Meenakshi Arora (The University of Alabama) for the use of her Anton Paar Modular Compact Rheometer (MCR) 302 instrument, Dr. Kimberly Lackey (The University of Alabama) for assistance with SEM, and Dr. Ken Belmore (The University of Alabama) for assistance with NMR spectroscopy.

Appendix A. Supplementary data

Supplementary data to this article can be found online at https://doi.org/10.1016/j.ijbiomac.2024.134493.

References

[1] M. Sepantafar, R. Maheronnaghsh, H. Mohammadi, F. Radmanesh, M.M. Hasani-Sadrabadi, M. Ebrahimi, H. Baharvand, Engineered hydrogels in cancer therapy and diagnosis, Trends Biotechnol. 35 (11) (2017) 1074–1087.

[2] K. Fernando, L.G. Kwang, J.T.C. Lim, E.L.S. Fong, Hydrogels to engineer tumor microenvironments in vitro, Biomater. Sci. 9 (7) (2021) 2362–2383.

[3] O. Habanjar, M. Diab-Assaf, F. Caldefie-Chezet, L. Delort, 3D cell culture systems: tumor application, advantages, and disadvantages, Int. J. Mol. Sci. 22 (22) (2021) 12200.

[4] A. Nyga, U. Cheema, M. Loizidou, 3D tumour models: novel in vitro approaches to cancer studies, Journal of Cell Communication and Signaling 5 (3) (2011) 239–248.

[5] Y. Ma, T. Han, Q. Yang, J. Wang, B. Feng, Y. Jia, Z. Wei, F. Xu, Viscoelastic cell microenvironment: hydrogel-based strategy for recapitulating dynamic ECM mechanics, Adv. Funct. Mater. 31 (24) (2021) 2100848.

[6] S. Tang, B.M. Richardson, K.S. Anseth, Dynamic covalent hydrogels as biomaterials to mimic the viscoelasticity of soft tissues, Prog. Mater. Sci. 120 (2021) 100738.

[7] O. Chaudhuri, Viscoelastic hydrogels for 3D cell culture, Biomater. Sci. 5 (8) (2017) 1480–1490.

[8] C.T. Mierke, Viscoelasticity acts as a marker for tumor extracellular matrix characteristics, Frontiers in Cell and Developmental Biology 9 (2021).

[9] K.M. Park, S. Gerecht, Polymeric hydrogels as artificial extracellular microenvironments for cancer research, Eur. Polym. J. 72 (2015) 507–513.

[10] J. Thakor, S. Ahadian, A. Niakan, E. Banton, F. Nasrollahi, M.M. Hasani-Sadrabadi, A. Khademhosseini, Engineered hydrogels for brain tumor culture and therapy, Bio-Des. Manuf. 3 (2020) 203–226.

[11] R.V. Kondapaneni, S.K. Gurung, P.S. Nakod, K. Goodarzi, V. Yakati, N.A. Lenart, S. S. Rao, Glioblastoma mechanobiology at multiple length scales, Biomaterials Advances 160 (2024) 213860.

[12] C. Vitale, M. Marzagalli, S. Scaglione, A. Dondero, C. Bottino, R. Castriconi, Tumor microenvironment and hydrogel-based 3D Cancer models for in vitro testing immunotherapies, Cancers 14 (4) (2022) 1013.

[13] G.F. Beeghly, K.Y. Amofa, C. Fischbach, S. Kumar, Regulation of tumor invasion by the physical microenvironment: lessons from breast and brain Cancer, Annu. Rev. Biomed. Eng. 24 (Volume 24, 2022) (2022) 29–59.

[14] A.A. Narkhede, J.H. Crenshaw, R.M. Manning, S.S. Rao, The influence of matrix stiffness on the behavior of brain metastatic breast cancer cells in a biomimetic hyaluronic acid hydrogel platform, J. Biomed. Mater. Res. A 106 (7) (2018) 1832–1841.

[15] K. Goodarzi, S.S. Rao, Hyaluronic acid-based hydrogels to study cancer cell behaviors, J. Mater. Chem. B 9 (31) (2021) 6103–6115.

[16] K. Goodarzi, R. Lane, S.S. Rao, Varying the RGD concentration on a hyaluronic acid hydrogel influences dormancy versus proliferation in brain metastatic breast cancer cells, J. Biomed. Mater. Res. A.

[17] J. Sievers, V. Mahajan, P.B. Welzel, C. Werner, A. Taubenberger, Precision hydrogels for the study of Cancer cell Mechanobiology, Adv. Healthc. Mater. 12 (14) (2023) 2202514.

[18] K.Y. Amofa, K.M. Patterson, J. Ortiz, S. Kumar, Dissecting TGF-β-induced glioblastoma invasion with engineered hyaluronic acid hydrogels, APL bioengineering 8 (2) (2024).

[19] E.M. Carvalho, E.A. Ding, A. Saha, A. Weldy, P.-J.H. Zushin, A. Stahl, M.K. Aghi, S. Kumar, Viscoelastic high-molecular-weight hyaluronic acid hydrogels support rapid glioblastoma cell invasion with leader-follower dynamics, bioRxiv (2024) 2024.04.04.588167.

[20] M.J. Duffy, T.M. Maguire, A. Hill, E. McDermott, N. O'Higgins, Metalloproteinases: role in breast carcinogenesis, invasion and metastasis, Breast Cancer Res. 2 (4) (2000) 1–6.

[21] E.S. Radisky, D.C. Radisky, Matrix metalloproteinases as breast cancer drivers and therapeutic targets, Front Biosci (Landmark Ed) 20 (7) (2015) 1144–1163.

[22] M. Ham, A. Moon, Inflammatory and microenvironmental factors involved in breast cancer progression, Arch. Pharm. Res. 36 (12) (2013) 1419–1431.

[23] Z. Balion, E. Sipailaite, G. Stasyte, A. Vailionyte, A. Mazetyte-Godiene, I. Seskeviciute, R. Bernotiene, J. Phopase, A. Jekabsone, Investigation of Cancer cell migration and proliferation on synthetic extracellular matrix peptide hydrogels, Front. Bioeng. Biotechnol. 8 (2020).

[24] Y. Rong, Z. Zhang, C. He, X. Chen, Matrix metalloproteinase-sensitive poly (ethylene glycol)/peptide hydrogels as an interactive platform conducive to cell proliferation during 3D cell culture, SCIENCE CHINA Technol. Sci. 64 (6) (2021) 1285–1294.

[25] S.S. Nazari, A.D. Doyle, K.M. Yamada, Mechanisms of basement membrane Micro-perforation during Cancer cell invasion into a 3D collagen gel, Gels 8 (9) (2022) 567.

[26] A.J. Berger, K.M. Linsmeier, P.K. Kreeger, K.S. Masters, Decoupling the effects of stiffness and fiber density on cellular behaviors via an interpenetrating network of gelatin-methacrylate and collagen, Biomaterials 141 (2017) 125–135.

[27] S.A. Fisher, P.N. Anandakumaran, S.C. Owen, M.S. Shoichet, Tuning the microenvironment: click-crosslinked hyaluronic acid-based hydrogels provide a platform for studying breast Cancer cell invasion, Adv. Funct. Mater. 25 (46) (2015) 7163–7172.

[28] S. Pradhan, J.H. Slater, Tunable hydrogels for controlling phenotypic cancer cell states to model breast cancer dormancy and reactivation, Biomaterials 215 (2019) 119177.

[29] K.L. Wiley, B.P. Sutherland, B.A. Ogunnaike, A.M. Kloxin, Rational Design of Hydrogel Networks with dynamic mechanical properties to mimic matrix remodeling, Adv. Healthc. Mater. 11 (7) (2022) 2101947.

[30] C. Wang, X. Tong, X. Jiang, F. Yang, Effect of matrix metalloproteinase-mediated matrix degradation on glioblastoma cell behavior in 3D PEG-based hydrogels, J. Biomed. Mater. Res. A 105 (3) (2017) 770–778.

[31] C. Wang, X. Tong, F. Yang, Bioengineered 3D brain tumor model to elucidate the effects of matrix stiffness on glioblastoma cell behavior using PEG-based hydrogels, Mol. Pharm. 11 (7) (2014) 2115–2125.

[32] C. Wang, S. Sinha, X. Jiang, L. Murphy, S. Fitch, C. Wilson, G. Grant, F. Yang, Matrix stiffness modulates patient-derived glioblastoma cell fates in three-dimensional hydrogels, Tissue Eng. Part A 27 (5–6) (2021) 390–401.

[33] A.A. Narkhede, J.H. Crenshaw, D.K. Crossman, L.A. Shevde, S.S. Rao, An in vitro hyaluronic acid hydrogel based platform to model dormancy in brain metastatic breast cancer cells, Acta Biomater. 107 (2020) 65–77.

[34] K.R. Coogan, P.T. Stone, N.D. Sempertegui, S.S. Rao, Fabrication of micro-porous hyaluronic acid hydrogels through salt leaching, Eur. Polym. J. 135 (2020) 109870.

[35] K. Goodarzi, F. Jonidi Shariatzadeh, A. Solouk, S. Akbari, H. Mirzadeh, Injectable drug loaded gelatin based scaffolds as minimally invasive approach for drug delivery system: CNC/PAMAM nanoparticles, Eur. Polym. J. 139 (2020) 109992.

[36] T. Canal, N.A. Peppas, Correlation between mesh size and equilibrium degree of swelling of polymeric networks, J. Biomed. Mater. Res. 23 (10) (1989) 1183–1193.

[37] P.J. Flory, J. Rehner Jr., Statistical mechanics of cross-linked polymer networks II, Swelling, The journal of chemical physics 11 (11) (1943) 521–526.

[38] B. Ananthanarayanan, Y. Kim, S. Kumar, Elucidating the mechanobiology of malignant brain tumors using a brain matrix-mimetic hyaluronic acid hydrogel platform, Biomaterials 32 (31) (2011) 7913–7923.

[39] W. Xiao, R. Zhang, A. Sohrabi, A. Ehsanipour, S. Sun, J. Liang, C.M. Walthers, L. Ta, D.A. Nathanson, S.K. Seidlits, Brain-mimetic 3D culture platforms allow investigation of cooperative effects of extracellular matrix features on therapeutic resistance in glioblastoma, Cancer Res. 78 (5) (2018) 1358–1370.

[40] J.B. Leach, C.E. Schmidt, Characterization of protein release from photocrosslinkable hyaluronic acid-polyethylene glycol hydrogel tissue engineering scaffolds, Biomaterials 26 (2) (2005) 125–135.

[41] A.L. Helling, E.K. Tsekoura, M. Biggs, Y. Bayon, A. Pandit, D.I. Zeugolis, In vitro enzymatic degradation of tissue grafts and collagen biomaterials by matrix metalloproteinases: improving the collagenase assay, ACS Biomater Sci. Eng. 3 (9) (2017) 1922–1932.

[42] X. Ma, J. Deng, Y. Du, X. Li, D. Fan, C. Zhu, J. Hui, P. Ma, W. Xue, A novel chitosan–collagen-based hydrogel for use as a dermal filler: initial in vitro and in vivo investigations, J. Mater. Chem. B 2 (18) (2014) 2749–2763.

[43] C.B. Rodell, R.J. Wade, B.P. Purcell, N.N. Dusaj, J.A. Burdick, Selective Proteolytic Degradation of Guest–Host Assembled, Injectable Hyaluronic Acid Hydrogels, ACS Biomaterials Science & Engineering 1(4) (2015) 277–286.

[44] R.V. Kondapaneni, R. Warren, S.S. Rao, Low dose chemotherapy induces a dormant state in brain metastatic breast cancer spheroids, AICHE J. 68 (12) (2022) e17858.

[45] R.V. Kondapaneni, S.S. Rao, Matrix stiffness and cluster size collectively regulate dormancy versus proliferation in brain metastatic breast cancer cell clusters, Biomater. Sci. 8 (23) (2020) 6637–6646.

[46] R.V. Kondapaneni, L.A. Shevde, S.S. Rao, A biomimetic hyaluronic acid hydrogel models mass dormancy in brain metastatic breast Cancer spheroids, Advanced Biology 7 (1) (2023) 2200114.

[47] R.V. Kondapaneni, S.K. Gurung, L.A. Shevde, S.S. Rao, Protocol for generating dormant human brain metastatic breast cancer spheroids in vitro, STAR Protocols 5 (2) (2024) 102962.

[48] P.S. Nakod, Y. Kim, S.S. Rao, Three-dimensional biomimetic hyaluronic acid hydrogels to investigate glioblastoma stem cell behaviors, Biotechnol. Bioeng. 117 (2) (2020) 511–522.

[49] M.S. Rehmann, K.M. Skeens, P.M. Kharkar, E.M. Ford, E. Maverakis, K.H. Lee, A. M. Kloxin, Tuning and predicting mesh size and protein release from step growth hydrogels, Biomacromolecules 18 (10) (2017) 3131–3142.

[50] J. Xia, Z.-Y. Liu, Z.-Y. Han, Y. Yuan, Y. Shao, X.-Q. Feng, D.A. Weitz, Regulation of cell attachment, spreading, and migration by hydrogel substrates with independently tunable mesh size, Acta Biomater. 141 (2022) 178–189.

[51] L.G. Treloar, The Physics of Rubber Elasticity, 1975.

[52] O. Jeon, S.J. Song, K.-J. Lee, M.H. Park, S.-H. Lee, S.K. Hahn, S. Kim, B.-S. Kim, Mechanical properties and degradation behaviors of hyaluronic acid hydrogels cross-linked at various cross-linking densities, Carbohydr. Polym. 70 (3) (2007) 251–257.

[53] D. Seliktar, A.H. Zisch, M.P. Lutolf, J.L. Wrana, J.A. Hubbell, MMP-2 sensitive, VEGF-bearing bioactive hydrogels for promotion of vascular healing, Journal of Biomedical Materials Research Part A 68A (4) (2004) 704–716.

[54] J. Kim, Y. Park, G. Tae, K.B. Lee, S.J. Hwang, I.S. Kim, I. Noh, K. Sun, Synthesis and characterization of matrix metalloprotease sensitive-low molecular weight hyaluronic acid based hydrogels, J. Mater. Sci. Mater. Med. 19 (2008) 3311–3318.

[55] V.P. Ribeiro, J. Silva-Correia, C. Gonçalves, S. Pina, H. Radhouani, T. Montonen, J. Hyttinen, A. Roy, A.L. Oliveira, R.L. Reis, Rapidly responsive silk fibroin hydrogels as an artificial matrix for the programmed tumor cells death, PloS One 13 (4) (2018) e0194441.

[56] T.D. Pollard, J.A. Cooper, Actin, a central player in cell shape and movement, science 326 (5957) (2009) 1208–1212.

[57] R. Dominguez, K.C. Holmes, Actin structure and function, Annu. Rev. Biophys. 40 (2011) 169–186.

[58] M. Izdebska, W. Zielińska, M. Hałas-Wiśniewska, A. Grzanka, Involvement of actin and actin-binding proteins in carcinogenesis, Cells 9 (10) (2020).

[59] S. Brayford, G. Schevzov, J. Vos, P. Gunning, The role of the actin cytoskeleton in cancer and its potential use as a therapeutic target, The cytoskeleton in health and disease (2015) 373–391.